Available online at www.sciencedirect.com

SciVerse ScienceDirect

Geochimica et Cosmochimica Acta 86 (2012) 196–213

Geochimica et Cosmochimica Acta

www.elsevier.com/locate/gca

A thermodynamic model for the system SiO_2–H_2O near the upper critical end point based on quartz solubility experiments at 500–1100 °C and 5–20 kbar

Jonathan D. Hunt [a,b,*], Craig E. Manning [b]

[a] Lawrence Livermore National Laboratory, Livermore, CA 94550, USA
[b] Department of Earth and Space Sciences, University of California, Los Angeles, CA 90095-1567, USA

Received 10 October 2011; accepted in revised form 2 March 2012; available online 20 March 2012

Abstract

A thermodynamic model of SiO_2–H_2O mixing in sub- and supercritical fluids has been developed based on new and existing experimental data on the solubility of quartz in H_2O. To supplement previously published data, we conducted new solubility experiments at 15 and 20 kbar and 900–1100 °C using hydrothermal piston–cylinder methods. At concentrations below ~10 mol% SiO_2, solubility was measured by single-crystal weight loss. At higher concentrations, solubility was determined by bracketing the presence and absence of quartz in quenched charges using multiple isothermal and isobaric runs with varying SiO_2–H_2O ratios. These data were combined with previously published results to construct a thermodynamic model of SiO_2–H_2O mixing. Following studies of silicate melts, the model takes oxygen in the fluid to be in three forms: free, molecular H_2O, Si-bridging oxygens (O^{2-}_{br}), and the terminal hydroxyls (OH^-_{tm}) of silanol groups. The equilibrium exchange of oxygen between these forms can be written $\frac{1}{2}H_2O + \frac{1}{2}O^{2-}_{br} = OH^-_{tm}$. The standard Gibbs free energy change of this reaction (ΔG°) was incorporated into a subregular solution model for mixing of SiO_2 liquid and H_2O fluid. The P–T dependences of ΔG° and interchange energies were derived by an error minimization algorithm, producing thirteen independent fit parameters. The model is applicable from 5 to 20 kbar and 500 °C to the dry melting curve of quartz. It reproduces experimentally derived quartz solubility data to 3.8% on average ($1\sigma = 5.3\%$). The model also predicts hydrous melting of quartz, critical melt–vapor mixing, activity–concentration relations, partial molar volume and entropy of aqueous silica, water speciation, and the thermal expansivity, isothermal compressibility, and isobaric heat capacity of a fluid in equilibrium with quartz. The model predicts a critical end point in the SiO_2–H_2O system at 1067 °C and 9.33 kbar, in very good agreement with the accepted location at ~1080 °C and 9.5–10 kbar. The model is also in good agreement with previous estimates of the extent of silica polymerization. The results of this study clearly demonstrate that there is an explicit link between polymerization chemistry and critical mixing of silicate–H_2O solutions.

1. INTRODUCTION

Understanding the thermodynamics of mixing between silicate liquids and water at high pressure (P) and temperature (T) is of fundamental importance to studies of fluid–rock interaction in the lower crust and upper mantle (Manning, 2004; Hack et al., 2007a,b). Owing to the low solubility of silicates in H_2O, lower and upper critical end points tend to exist on their solubility and hydrous melting curves. Although the P and T of lower critical end points differ little from the critical point of pure H_2O, upper critical end points vary widely, and may exert important controls on geologic systems. For example, at pressures greater than the pressure of an upper critical end point, mineral solubility increases continuously as T increases,

* Corresponding author at: Lawrence Livermore National Laboratory, Livermore, CA 94550, USA. Tel.: +1 310 487 3864.
E-mail addresses: hunt50@llnl.gov, jonathan.david.hunt@gmail.com (J.D. Hunt).

0016-7037/$ - see front matter © 2012 Elsevier Ltd. All rights reserved.
http://dx.doi.org/10.1016/j.gca.2012.03.006

allowing fluids with subequal silicate and water contents to be in equilibrium with the surrounding rock. Fluids of these intermediate compositions may play a key role in transport of material in subduction zones (Manning, 2004). Significant effort has been made in establishing the locations of critical end points in geologically relevant systems (Kennedy et al., 1962; Shen and Keppler, 1997; Bureau and Keppler, 1999; Stalder et al., 2000; Sowerby and Keppler, 2002; Mibe et al., 2004, 2007, 2011; Kessel et al., 2005a,b; Hermann and Spandler, 2008; Newton and Manning, 2008); however, the thermodynamic and transport properties of silicate–water systems, especially around the upper critical end point, remain poorly constrained (Hack et al., 2007a,b; Audétat and Keppler, 2004; Hack and Thompson, 2011).

Silica is a major rock-forming oxide of the earth's crust and mantle, and it is among the most soluble oxides in H_2O at crustal and upper mantle conditions (Manning, 1994). Silica's high concentration and primary role in controlling solute structure (Mysen, 1998, 2010a) make the binary SiO_2–H_2O an essential foundation for understanding silicate–water binary systems. Early experimental studies of quartz solubility (e.g., Kennedy, 1950) found that quartz has low solubility at low P and T near the critical point of water, implying that the P and T conditions of the lower critical end point of the SiO_2–H_2O system are not far removed from those of the critical point of pure water. There have been numerous models of quartz solubility along the H_2O steam curve, and to conditions of medium-grade crustal metamorphism (5 kbar, 600 °C; e.g., Walther and Helgeson, 1977, and references therein).

At P and T above 5 kbar and 600 °C, the solubility of quartz in H_2O increases considerably (Anderson and Burnham, 1965; Manning, 1994). Empirical relationships to describe this increase in quartz solubility were developed by Fournier and Potter (1982), Manning (1994), and Dolejs and Manning (2010). In these studies, quartz solubility was correlated with the specific volume or density of pure water. Manning (1994) and Dolejs and Manning (2010) found that quartz solubility below 900 °C and 20 kbar could be described by a linear correlation of log SiO_2 molality with log H_2O density. These studies successfully predict quartz solubility over a wide range of P and T, but become inaccurate as the hydrous melting point is approached ($\geqslant$900 °C) because of a rapid increase in solubility at higher T.

The formulations of SiO_2 solubility in H_2O by Walther and Helgeson (1977), Fournier and Potter (1982), Manning (1994), and Dolejs and Manning (2010) do not account for two key, interrelated aspects of the chemistry of aqueous silica: polymerization (e.g., Iler, 1979) and critical behavior (Kennedy et al., 1962). While silica polymerization has long been known in aqueous solutions at low temperature, Zotov and Keppler (2000, 2002) and Newton and Manning (2002, 2003) presented the first evidence for the polymerization of aqueous SiO_2 at high P and T. In these studies, speciation models were derived assuming the presence of two species: $Si(OH)_4$ monomers and $Si_2O(OH)_6$ dimers. While the models provide constraints on silica activity and speciation, they are not applicable at concentrations above ~2 m (3.4 mol%), where additional polymeric species and the deviation of water activity from unity becomes significant (Newton and Manning, 2008). Gerya et al. (2005) attempted to take further polymerization into account by assuming that successive SiO_4^{4-} attachments to a polymer have the same equilibrium constant as the dimer-forming reaction. This model describes silica solubility quite well to 900 °C, and provides information on the speciation and activity of silica. However, it does not provide for melting or critical phenomena. Doltsinis et al. (2007) used ab initio molecular dynamics to show that various silica polymers are chemically stable on short time frames (5–10 ps), but computational limitations thus far preclude calculation of relative abundances of species.

The second feature of the system SiO_2–H_2O not adequately incorporated into previous models is the location of the hydrous melting curve and its termination in an upper critical end point. Kennedy et al. (1962) first determined the melting curve and proposed an upper critical end point at 9.7 kbar and 1080 °C, where quartz coexisted with a fluid containing ~50 mol% SiO_2. Quartz solubility determinations by Nakamura (1974) imply that the SiO_2–H_2O system is supercritical at 15 kbar, 900–1400 °C, in agreement with Kennedy et al. (1962). Although the existence of the end point was challenged by Stewart (1967) and Mysen (1998), the original finding of Kennedy et al. (1962) has now been confirmed by Newton and Manning (2008). General phase relations in the SiO_2–H_2O system consistent with these results are shown in Fig. 1.

In silicate–H_2O systems, the positions of hydrothermal melting curves and their end points depend strongly on the nature and extent of polymerization of aqueous silicate species, which increase dramatically in abundance as melting is approached (Manning, 2004; Newton and Manning, 2008; Manning et al., 2010). Any model that seeks to combine solubility and melting behavior in the system SiO_2–H_2O must therefore account explicitly for silica polymerization in the aqueous phase. Using a subregular mixing model involving monomers, dimers, and higher order polymers, Newton and Manning (2008) predicted the speciation of silica at 1080 °C and 10 kbar. They found that nearly 80% of the silica in solution in equilibrium with quartz was contained in higher-order polymers. This model describes supercritical solubility and activity–concentration relations, but only at a single pressure and temperature near the upper critical end point.

In the present work, we seek to extend this approach by formulating a model for the SiO_2–H_2O system that explains quantitatively the solubility of stable and metastable SiO_2-bearing phases, the speciation of aqueous and molten SiO_2, activity–concentration relations (and therefore physical properties based on the derivatives of activity), and stable and metastable fluid immiscibility.

To determine mixing properties of the SiO_2–H_2O system over a much broader pressure region more quantitatively, we conducted new experiments on quartz solubility in H_2O between 900 and 1100 °C at 15 and 20 kbar. The new results provide data that, in conjunction with previous quartz solubility studies, constrain the first quantitative thermodynamic model of SiO_2–H_2O mixing capable of accurately describing quartz solubility, critical behavior,

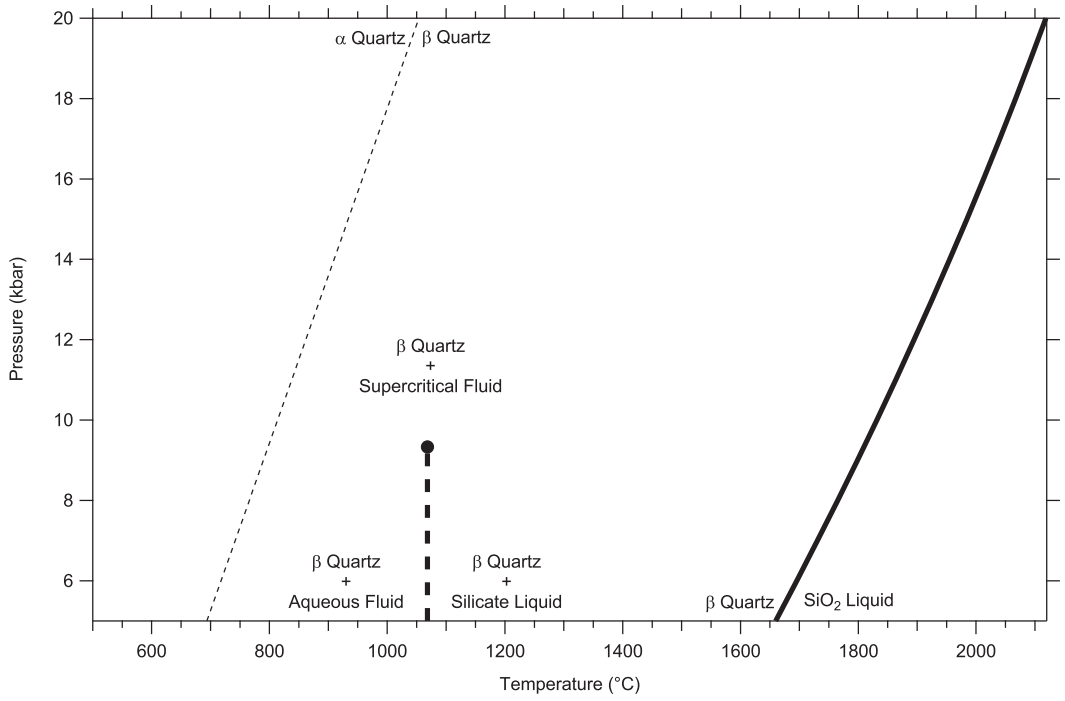

Fig. 1. General phase relations in the SiO_2–H_2O systems within the relevant *PT* region of the model of this study. The solid bold curve is the dry quartz melting curve, calculated from Jackson (1976). The dashed bold curve is the hydrous melting curve, terminating at the upper critical end point (this study). The thin dashed curve is the transition from α to β quartz, calculated from Holland and Powell (1998) (2002 update).

activity–composition relations, and speciation at high *P* and *T*.

2. EXPERIMENTAL METHODS

Due to the wide solubility range investigated in this study, two types of experiments were conducted: single-crystal solubility runs at low SiO_2 concentration (SC experiments, Table 1), and phase-bracketing runs at high SiO_2 concentration (PB experiments, Table 1). For the single-crystal solubility runs, starting materials were ultrapure H_2O and a polished fragment of natural Brazilian quartz (Manning, 1994; Newton and Manning, 2008). Where quartz solubility was higher than SiO_2 mole fraction $>\sim 0.1$, use of a single quartz crystal was not feasible (Newton and Manning, 2008). Instead, finely ground quartz from the same source was used in multiple isothermal and isobaric phase-bracketing runs at different SiO_2

Table 1
Experimental results.

Run	Type	*P* (kbar)	*T* (°C)	Time (h)	H_2O in (mg)	Quartz in (mg)	Quartz out (mg)	X_s
1	SC	15	900	2.5	26.211	6.521	0.854	0.0609
2	SC	15	900	20	24.634	6.091	0.741	0.0611
7	SC	15	950	3	24.230	13.450	5.136	0.0933
5	PB	15	1000	3	22.023	14.908	–	>0.1687
10	PB	15	1000	3	16.660	12.138	+	<0.1793
9	PB	15	1050	2.5	19.730	29.859	1.5 + tr	0.3012
3	SC	20	900	17.5	22.480	7.594	1.669	0.0732
11	PB	20	950	1.5	18.644	8.958	+	<0.1259
12	PB	20	950	1.5	20.032	8.553	–	>0.1135
13	PB	20	1000	1.5	20.209	18.237	–	>0.2130
14	PB	20	1000	1.5	21.988	24.778	+	<0.2525
16	PB	20	1100	1	9.480	31.241	–	>0.4970
18	PB	20	1100	1	4.802	19.458	+	<0.5485

Abbreviations: SC, single quartz crystal; PB, phase bracketing. In the quartz-out column, numerical entries indicate the weight of a single weighable quartz crystal, a plus sign indicates the presence of irretrievable fine grained quartz, tr indicates a negligible amount of fine grained quartz, and a dash indicates a lack of quartz. Maximum uncertainty in reported SiO_2 mole fraction (X_s) is 0.0001, based on propagation of weighing errors.

concentrations to identify the quartz saturation composition. In both SC and PB experiments, starting materials were sealed by arc-welding in a single, 1.5 cm-long Pt tube (3.5 mm O.D., 0.15 mm wall thickness), with negligible loss of H_2O upon sealing (Newton and Manning, 2006, 2007; Tropper and Manning, 2007a,b).

All experiments were carried out in a piston–cylinder apparatus using 2.54 cm-diameter furnaces with graphite heater sleeves and NaCl pressure medium (Manning and Boettcher, 1994). The experiments were conducted in the temperature range 900–1100 °C (±3 °C) and the pressure range 15–20 kbar (±0.3 kbar). Temperature was measured and controlled by type S thermocouples. No correction was made for the effect of pressure on emf. Experiments were quenched to <200 °C in less than 12 s by shutting off the heating power. A Mettler M3 microbalance with a reproducibility of ±2 μg (1σ) was used to weigh quartz crystals before and after SC experiments, as well as initial and final H_2O. Final H_2O weight was measured by loss upon drying, and was used solely as a check against water loss during the experimental run. In PB experiments, due to the high proportion of initial silica, a significant amount of H_2O becomes structurally bound in the vapor quench phase, and the H_2O weight after the experiment cannot be measured by loss upon drying. Therefore, only initial weights were recorded for PB experiments. Propagation of weighing errors leads to a maximum error in silica mole fraction (X_s) of 0.0001 (1σ). At a given P and T, PB experiments were repeated until bracket width was $X_s \sim 0.05$ to sufficiently constrain the thermodynamic model. Only the most tightly limiting experiments are reported.

3. RESULTS

Experimental results are given in Table 1 and Fig. 2. Upon quenching and drying of the experimental charges, soluble silica was identified in the run products as an amorphous, chalky or glassy matrix. Evidence of coexisting, immiscible fluids such as the presence of large, discrete glass spheres (e.g., Antignano and Manning, 2008) was not observed, indicating that all runs were in the supercritical SiO_2–H_2O region. Residual quartz in the phase bracketing runs was distinguished from soluble silica in the run products by its birefringence using optical microscopy. It occurred as rounded, subhedral to euhedral crystals <100 μm in diameter embedded in the chalky or glassy matrix. Quartz crystals from SC experiments were found to be subhedral to euhedral as well.

To determine the time required for equilibrium, experiments were performed for 2.5 and 20 h at the lowest temperature and pressure investigated (900 °C, 15 kbar). The final quartz crystal was subhedral in the 2.5 h run, but euhedral after the 20 h run; however, the two experiments show negligible difference in solubility, suggesting that equilibrium is achieved within 2.5 h. Solubilities at <1050 °C, 15 kbar were found to be systematically higher than those measured by Nakamura (1974) (Fig. 2). This may be because Nakamura's short run times (~30 min) did not allow the system to fully equilibrate below 1050 °C. In contrast, agreement between the data from Nakamura (1974) and the current study at 1050 °C imply that equilibrium is achieved within ~30 min at >1050 °C.

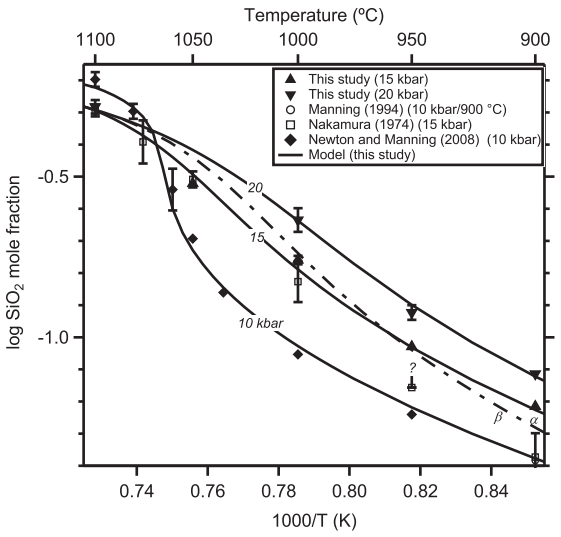

Fig. 2. Variation in quartz solubility in H_2O as a function of temperature. Solid curves show solubility isobars, based on the thermodynamic model created from the data from this study, Newton and Manning (2000, 2008), Manning (1994), and Nakamura (1974). The 1σ weighing errors from the present study are smaller than the symbol size. Data points with visible error bars reflect the midpoints of bracketing experiments, shown by the error bars. The dash-dot curve is the α–β quartz inversion (Cohen and Klement, 1967).

The new data indicate that below ~1050 °C, quartz solubility at 15 and 20 kbar is significantly higher than at 10 kbar. For example, at 1000 °C, quartz solubility climbs from 8.85 mol% at 10 kbar (Newton and Manning, 2008) to 17.4 ± 0.53 mol% at 15 kbar and to 23.28 ± 1.98 mol% at 20 kbar. In contrast, at 1050–1100 °C, quartz solubility at both 15 and 20 kbar is lower than the solubility at 10 kbar, so that at 1100 °C, quartz solubility drops from 63.59 ± 3.36 mol% at 10 kbar (Newton and Manning, 2008) to 50.9 ± 2.2 mol% at 15 (Nakamura, 1974) and 52.28 ± 2.58 mol% at 20 kbar (this study).

Our results are consistent with those of Newton and Manning (2008). As P increases from 10 to 20 kbar, tangents to the isobaric solubility curves become progressively shallower at constant, ~critical T of 1050–1080 °C (Fig. 2), indicating that P is increasing in excess of an upper critical end point. The intersection of the 15 and 20 kbar solubility curves at ~1100 °C suggests that the intersection of the 15 and 10 kbar solubility curves may occur at a lower concentration of silica (and slightly lower T) than the intersection of the 20 and 10 kbar solubility curves (Fig. 2). This has important implications for near-critical solubility topology (see below).

4. DISCUSSION

4.1. Modeling solubility and activity–concentration relations

The equation of Manning (1994) accurately describes quartz solubility between 500 and 900 °C up to 10 kbar,

and between 500 and 700 °C from 10 to 20 kbar. The monomer + dimer model of Newton and Manning (2002, 2003) describes silica activity in relatively dilute solutions (<2 m). However, neither the equation of Manning (1994) nor the activity model of Newton and Manning (2002, 2003) is applicable at the high silica concentrations reached as P and T increase further. For example, the equation of Manning (1994) under-predicts quartz solubility at 900 °C between 10 and 20 kbar by ~15–30%. In an attempt to model silica activity–concentration relations in the high concentration region near the upper critical end point, Newton and Manning (2008) proposed a subregular solution to describe the isobaric, isothermal behavior of the quartz-water system at 1080 °C and 10 kbar. An alternative solution model must be employed to fully describe the solubility of quartz over a range of P and T.

Ideal, regular, and subregular mixing models are advantageous for their numerical simplicity, but they are strictly applicable to solutions of non-interacting to weakly interacting particles. Without modification, they are not appropriate for solutions with components that interact strongly to form chemical complexes. In the case of the SiO_2–H_2O system specifically, a subregular solution cannot take into account the strong chemical interaction in the fluid associated with oxygen exchange between free H_2O, bridging O^{2-} in polymerized silicate species, and terminal OH^- of silanol groups, represented by

$$\tfrac{1}{2}H_2O + \tfrac{1}{2}O^{2-}_{br} = OH^-_{tm} \quad (1)$$

where the subscripts br and tm refer, respectively, to bridging and terminal oxygen positions. Eq. (1) describes any aqueous oxide polymerization or depolymerization reaction, such as the dimer–monomer reaction $H_2O + Si_2O(OH)_6 = 2Si(OH)_4$, but on a single-oxygen basis. In principle, the SiO_2–H_2O system could be described by a regular or subregular solution of three components – H_2O, O^{2-}, and OH^-, with a term added to describe the additional free energy derived from creating the OH^- component, similar to the thermodynamics of liquid alloys (e.g., Singh et al., 1993). However, the three-component regular or subregular solution would require too many parameters to fit the available data.

We therefore employed a subregular solution between two components, SiO_2 and H_2O. We added an additional term to the subregular solution in order to describe the standard Gibbs free energy of the exchange of oxygen between Si-bridging positions and free water positions to hydroxyl positions; that is, OH^- formation by depolymerization via reaction 1 (ΔG°_1). The standard state for SiO_2 is taken to be unit activity of pure molten silica ($SiO_{2,liq}$), the standard state for quartz and H_2O is unit activity of the pure phase, and the standard state for bridging oxygens and terminal hydroxyls is the hypothetical unit mole fraction solution of the species referred to infinite dilution. We assume that the free energy of the formation of one OH^- group is independent of the total concentration of OH^- groups formed (X_{OH^-}); that is, the Gibbs free energy of each new OH^- is additive. Assuming that all non-ideality is accounted for by the two-component interchange energies, the activity of each species in Eq. (1) is equal to its mole fraction, which leads to

$$\frac{X_{OH^-}}{\sqrt{X_{H_2O}X_{O^{2-}}}} = K_1 = \exp\left(\frac{-\Delta G^\circ_1}{RT}\right) \quad (2)$$

where K_1 is the equilibrium constant for Eq. (1). At a given P, T, and silica mole fraction (X_s), the total and excess free energy of mixing (ΔG_{mix} and ΔG_{ex}, respectively) of SiO_2 and H_2O are given by:

$$\Delta G_{mix} = RT[X_s \ln(X_s) + (1 - X_s)\ln(1 - X_s)] + \Delta G_{ex} \quad (3)$$

$$\Delta G_{ex} = X_s(1 - X_s)(W_s(1 - X_s) + W_h X_s) - X_{OH^-} * \Delta G^\circ_1 \quad (4)$$

where W_s and W_h are interchange energies for $SiO_{2,liq}$ and H_2O, respectively. Because each unit of SiO_2 contains two oxygen atoms, and mass balance requires that each hydroxyl group created needs $\frac{1}{2}H_2O$ and $\frac{1}{2}O^{2-}$, the total number of oxygen atoms in the system, normalized by the sum of the moles of H_2O and SiO_2 in the system, is given by $1 + X_s$, the number of bridging oxygens present ($X_{O^{2-}}$) is given by $2X_s - \frac{1}{2}X_{OH^-}$, and the number of free water molecules (X_{H_2O}) is given by $1 - X_s - \frac{1}{2}X_{OH^-}$. Thus, at a given X_s, these three equations have three independent variables: W_s, W_h, and ΔG°_1, as X_{OH^-} can be calculated directly from Eq. (2) (see Appendix A).

The equations were solved by recognizing that, given the full expression for the Gibbs free energy of mixing in a binary SiO_2–H_2O fluid, the solubility of quartz at any given P and T is defined by a mechanical mixing line in G–X_s space between ΔG°_{quartz} and the composition in a mixed SiO_2–H_2O fluid that possesses the lowest ΔG in the presence of quartz. This composition can be found by numerically solving the equation of the following straight line in G–X_s space

$$(1 - X_s)\left.\frac{\partial \Delta G_{mix}}{\partial X_s}\right|_{X_s} + \Delta G_{mix}|_{X_s} + \Delta G^\circ_{Q\text{–}L} = 0 \quad (5)$$

for X_s subject to the condition that ΔG_{mix} between X_s and 1 is greater than the linear combination of $\Delta G_{mix}|_{X_s}$ and $\Delta G^\circ_{Q\text{–}L}$, where $\Delta G^\circ_{Q\text{–}L}$ denotes the standard Gibbs free energy of metastable melting of quartz, given by the approximation

$$\Delta G^\circ_{Q\text{–}L} = (T_{melt} - T)\Delta S^\circ_{Q\text{–}L} \quad (6)$$

where T_{melt} is the temperature of dry quartz melting from Jackson (1976), and $\Delta S^\circ_{Q\text{–}L}$ is taken to be 5.53 J/mol K (Richet et al., 1982), independent of P. It should be noted that correction of a numerical error of Newton and Manning (2008) means that use of this value of $\Delta S^\circ_{Q\text{–}L}$ and a metastable melting point of 1427 °C at one bar (Richet et al., 1982) does not produce the implausible ~100% volume of melting noted by Newton and Manning (2008), but rather ~10% (0.2 J/bar), a far more reasonable value. The activities of silica and water in the fluid (respectively, $a_{s,l}$ and a_h) can be computed from the modified subregular solution model, where

$$RT\ln a_{s,l} = RT\ln X_s + (1 - X_s)^2(W_s + 2X_s(W_h - W_s)) - \Delta G^\circ_1\left[X_{OH^-} + (1 - X_s)\frac{\partial X_{OH^-}}{\partial X_s}\right] \quad (7)$$

$$RT\ln a_h = RT\ln(1 - X_s) + X_s^2(W_h + 2(1 - X_s)(W_s - W_h)) - \Delta G^\circ_1\left[X_{OH^-} - X_s\frac{\partial X_{OH^-}}{\partial X_s}\right] \quad (8)$$

The activity of silica at quartz saturation ($a^{Q}_{s,l}$) can also be calculated from the depression of the melting point of quartz by H_2O (Newton and Manning, 2008), where

$$RT \ln a^{Q}_{s,l} = -\Delta G^{\circ}_{Q-L} = (T - T_{melt})\Delta S^{\circ}_{Q-L} \quad (9)$$

Activities calculated in this way are identical to activities calculated by the modified subregular solution model using model-derived solubilities. In other words, equating the right hand sides of Eqs. (7) and (9) leads to an expression that can be used to calculate X_s at quartz saturation (see Appendix A). This expression is algebraically equivalent to Eq. (5) when Eqs. (3) and (4) are substituted in Eq. (5) for ΔG_{mix} and the appropriate derivative is taken, recognizing that X_{OH^-} is a function of X_s. The mixing parameters and ΔG°_{1} can therefore be obtained by regression of experimentally obtained quartz solubility data ((Manning, 1994; Newton and Manning, 2000, 2003, 2008; Nakamura, 1974) (>1050 °C only); this study).

Non-linear least squares regression of these data with added interpolated points, gave:

$$\Delta G^{\circ}_{1} = 22070 - 19.08T - 1.3168p + 2.2987 \times 10^{-5}P^2 + 5.4464 \times 10^{-5}T^2 + 18.990 \times 10^{-3}PT \quad (10)$$

$$W_s = 92631 - 24.585T - 4.9086P + 9.1719 \times 10^{-5}P^2 \quad (11)$$

$$W_h = 110740 - 65.569T - 1.1141P \quad (12)$$

where T is in K, P is in bars, and energies are in Joules. The average absolute error between solubilities calculated by the model using these coefficients and experimental data is 3.8%, and the standard deviation of the error is 5.3% (1σ). Fig. 3 shows model errors as functions of P, T, and X_s. All but three data points are within 10% of the experimental value and 70% of the data points are within 5% of the experimental value. The resulting fit possesses thirteen independent parameters, nine of which are constant or linear in P or T. Considering that Manning (1994) and Dolejs and Manning (2010) required seven independent parameters to describe quartz solubility at lower P and T, it is encouraging that only six additional parameters are required to describe highly non-linear quartz solubility, including critical phenomena, over a larger PT region.

The current model is applicable only between temperatures of 500 °C and the dry melting point of quartz at pressures between 5 and 20 kbar. It does not accurately capture the observed linear correlation of quartz solubility with the density of water (Manning, 1994) at lower P and T. This behavior is most likely due to the strong non-ideality of the SiO_2–H_2O system at low P and T.

Model quartz-solubility values are shown in Fig. 4. The solubility isopleths broadly follow the schematic topology developed by Hack et al. (2007a,b); however, our isopleths show a slight curvature between 1050–1100 °C above 10 kbar, indicating that a local solubility minimum exists at ~15 kbar between 1065 and 1100 °C. This is a reflection of the experimental observation above that the intersection of the 15 and 20 kbar solubility curves occurs at ~1100 °C, while the intersection of each of those curves with the 10 kbar solubility curve occurs at a lower T and silica concentration. While this may seem counterintuitive, there is no a priori reason that isobaric solubility curves must intersect at the same temperature and composition. Given the uncertainties in the experimental measurements at 1100 °C, the size of this local solubility minimum in PTX space has a large uncertainty. However, given the experimental difficulties at such high quartz/water ratios, it is unlikely that a reasonable number of experiments will provide the precision necessary to determine the true nature of the relationship between the 10, 15, and 20 kbar solubility curves between 1065 and 1100 °C.

The predicted trace of the critical curve, defined as the locus of points in PT space above which (in either T or P) no stable or metastable fluid immiscibility exists (Fig. 4), is much steeper than that of Hack et al. (2007a,b); the model critical temperature at ~5–10 kbar pressure is therefore much lower than is estimated from topology. It is important to emphasize that the location of the critical curve is not directly constrained by experimental data.

Fig. 5 shows phase relations in four isobaric sections at various pressures. The model clearly captures the topological change from a stable miscibility gap in the subcritical region to the intersection of the crest of the miscibility gap (the critical temperature) with the solubility curve, which forms an upper critical end point on the hydrothermal melting curve, and the increasing metastability of the miscibility gap with rising pressure across the full binary. Experimental quartz solubilities are accurately reproduced; however, the model predicts a more H_2O-rich melt composition at 5 kbar, 1100 °C than was inferred by Kennedy et al. (see Section 4.3).

Fig. 6 shows the polythermal activity of silica and water at 10 kbar and the quartz saturation temperature from 500 to 1840 °C, in addition to the silica activities in undersaturated solutions at various temperatures. Allowing the parameters of the modified subregular solution vary with T yields nearly constant activity of silica at quartz saturation over a larger range of silica concentration (Fig. 6) than an isothermal subregular solution (Newton and Manning, 2008). It is significant that silica activity initially rises rapidly with increasing T at quartz saturation and then levels off to stay nearly constant. By using a dry silica melt as the standard state, the silica activity at quartz saturation is dependent solely on T (Eq. (9)). Therefore, the non-ideality of the activity curve in Fig. 6 is entirely due to the concentration of silica in the fluid at quartz saturation. At low T, silica concentration is low relative to silica activity, and the dissolved silica is largely monomeric. As T increases, an increasing amount of silica can be dissolved, most likely as more polymerized species, which lowers the slope of the activity curve and turns it horizontal as a very large amount of silica is dissolved over a small temperature range. This is supported by recent work in hydrothermal diamond anvil cells, which point to a rapid increase in the oligomer/monomer abundance ratio as either T increases at quartz saturation near 800 °C (Mysen, 2010a), or simply as the total concentration of silica in solution is increased at the same T (Hunt et al., 2011).

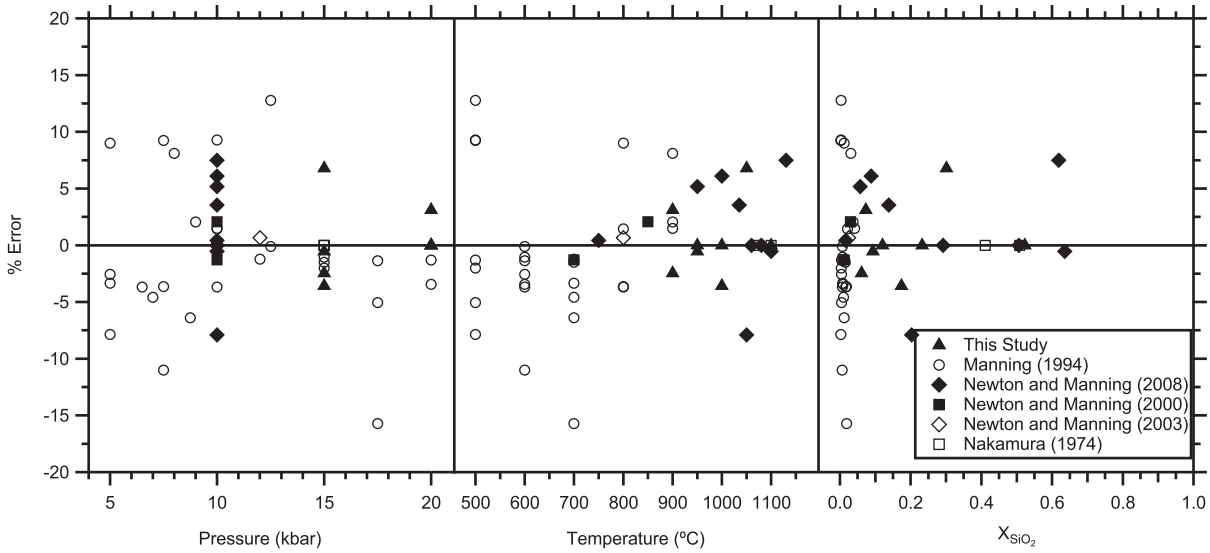

Fig. 3. Model agreement with experiment expressed as % error $(100(X_{\text{model}} - X_{\text{exp}})/X_{\text{exp}})$ as a function of pressure, temperature, and experimentally determined composition.

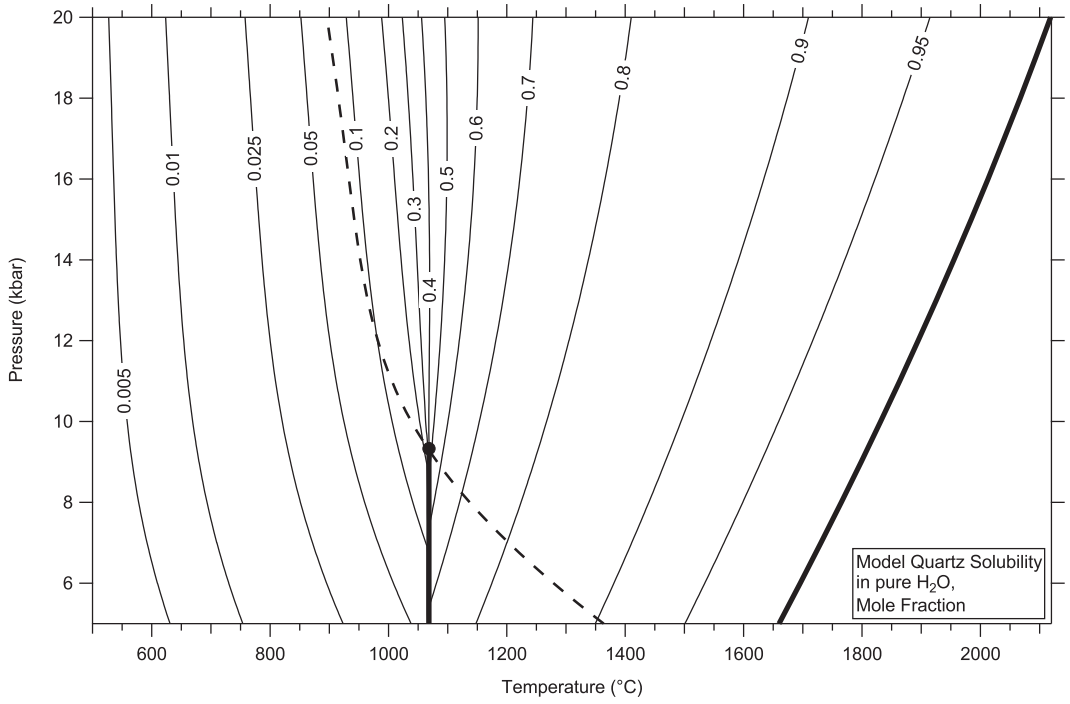

Fig. 4. Model variation in quartz solubility in H_2O as a function of temperature and pressure. Bold curves are the wet and dry melting curves of quartz. The dry melting curve is calculated from Jackson (1976), and the wet melting curve is calculated from the model of the present study. The bold dashed curve is the critical curve, stable above the wet melting temperature, and metastable below the wet melting temperature. The intersection of the wet melting curve with the critical curve defines the upper critical end point, determined by the model to be located at 9330 bars and 1067 °C. The lighter solid curves are contours of quartz solubility in mole fraction.

4.2. Hydration state of silica

Because the modified subregular solution model includes an explicit calculation of X_{OH^-}, it is possible to predict an average state of hydration (X_{OH^-}/X_s) of solutions at any given composition, P, and T. In this formulation, if $X_{OH^-}/X_s = 4$, then the solution is composed entirely of silica monomers, because each four-coordinated Si atom will be bonded to four terminal OH^- groups. Monomeric silica is also denoted as Q^0, because it is not bonded to other Si atoms through bridging oxygens. Similarly, $X_{OH^-}/X_s = 3$ corresponds to an average state of hydration equivalent to that of the dimer (Q^1), $X_{OH^-}/X_s = 2$ corresponds to rings and infinite chains (Q^2), $X_{OH^-}/X_s = 1$

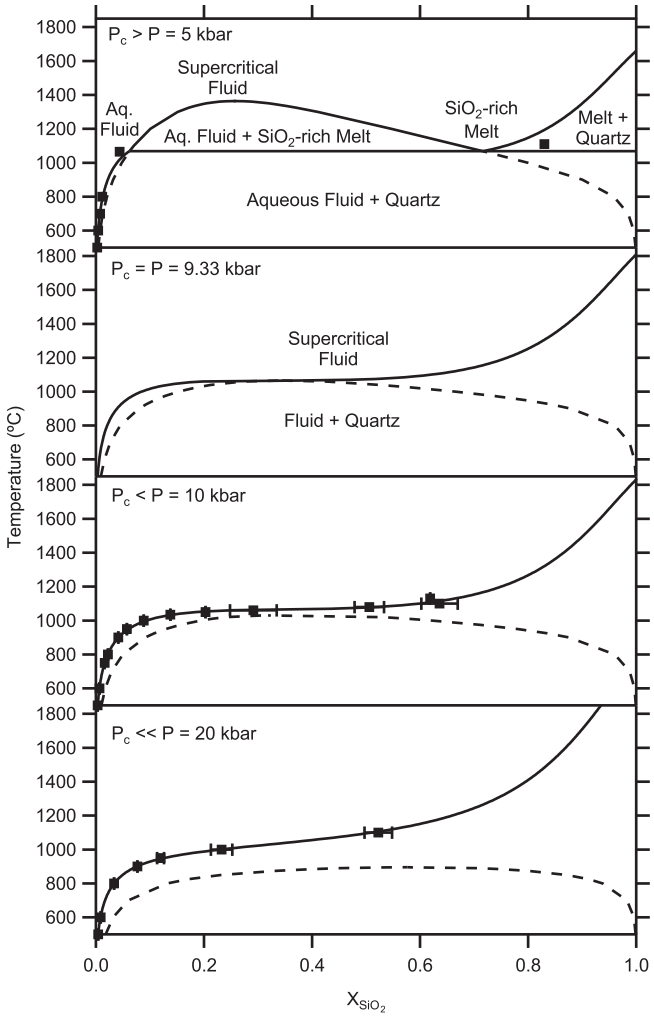

Fig. 5. Selected isobaric sections of quartz solubility and phase relations as a function of temperature and composition. Below the critical end point pressure (a), a stable miscibility gap exists between aqueous fluid and silicate melt. The intersection of the solubility curve with the miscibility gap defines the hydrous melting temperature. Below this temperature, the miscibility gap is metastable. At the critical end point pressure (b), the miscibility gap intersects the solubility curve at only one point, defining the critical end point composition where the solubility curve has a horizontal tangent. Just above the critical end point pressure (c), the miscibility gap is entirely metastable, and far above the critical end point pressure (d), the slope of the solubility curve increases so that the increase in solubility with increasing T is more gradual than at or near the critical end point pressure. Data points are experimental points from Manning (1994), Newton and Manning (2000, 2008), Kennedy et al. (1962), and this study.

to cages (Q^3), and $X_{OH^-}/X_s = 0$ to dry silica melt (Q^4). In this Q notation, Eq. (1) would be expressed as $\frac{1}{2}H_2O + Q^n = Q^{n-1}$.

The most important control on aqueous silica polymerization is the concentration of aqueous silica. Fig. 7 shows the partitioning of oxygen between H_2O, OH^-, and O^{2-} and the average hydration state of aqueous silica at 10 kbar and 1080 °C as a function of composition, which is represented by the number of oxygens provided by the water component divided by the total number of oxygens in the system. This representation of composition has the advantage of being independent of the number of oxygens per formula unit of silicate, which eases comparison of different systems (e.g., Stolper, 1982). While the most dilute solutions are predominantly monomeric, the average state of hydration drops to 1 as quartz saturation (~50 mol%) is reached. Newton and Manning (2008) determined that at quartz saturation at 10 kbar and 1080 °C, nearly 80% of the silica in solution is contained in "higher oligomers", defined as any silica species more highly polymerized than the dimer. If the present model and the model of Newton and Manning (2008) are both correct, the higher oligomers have an average state of hydration of 0.25, corresponding to a slightly hydrated melt. The structure of this fluid may in fact be similar to that of colloidal silica (e.g., Iler, 1979), with suspended, dry amorphous or molten silica surrounded by a hydrated layer in equilibrium with silica monomers and small oligomers. Assuming a dry amorphous or liquid silica density of 2.2–2.4, and that on average, surface tetrahedra are Q^3 species while interior tetrahedra are Q^4 species, an X_{OH^-}/X_s ratio of 0.25 is equivalent to silica colloids of approximately 8–9 nm diameter.

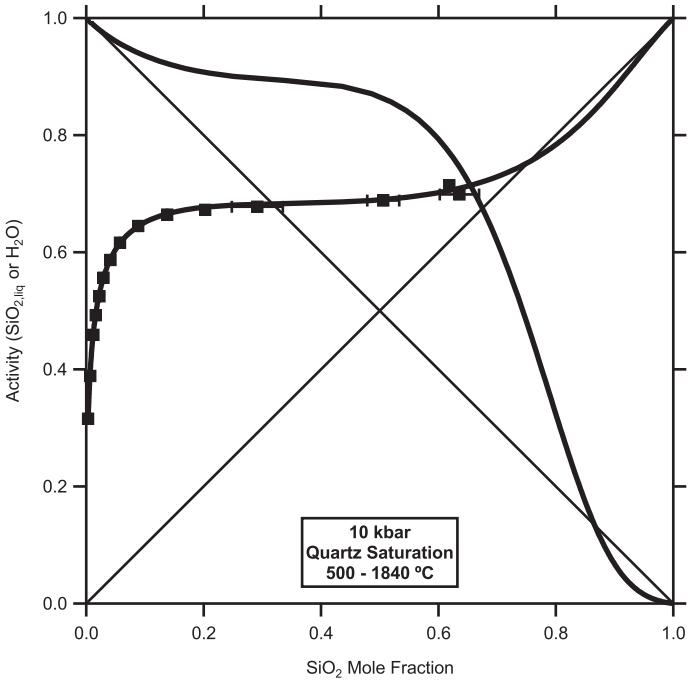

Fig. 6. Activity–concentration relations of SiO_2 and H_2O components in a quartz saturated aqueous fluid at 10 kbar, from 500 °C to the melting point of quartz. Filled squares are data points from Manning (1994) and Newton and Manning (2000, 2002, 2008), with activities calculated from the depression of the melting point of quartz in the presence of H_2O. The thin solid lines represent ideal mixing, while the solid curves show the model-derived activities of SiO_2 and H_2O. Because this diagram is polythermal with a minimum temperature of 500 °C, the activities for silica and water are not calculated at compositions less than the quartz saturation composition at 500 °C.

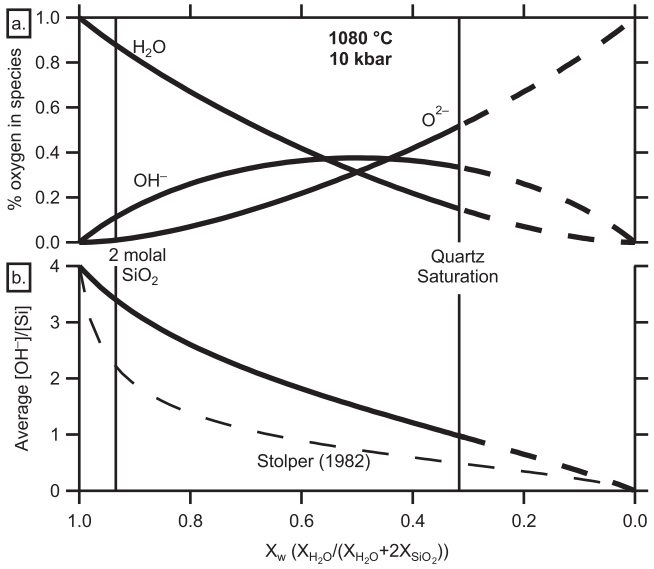

Fig. 7. (a) Partitioning of oxygen between H_2O, OH^-, and O^{2-} and (b) average state of hydration of solute silica (N_{OH^-}/X_s ratio) as a function of composition at 10 kbar and 1080 °C. Composition is represented by the number of oxygens provided by the water component divided by the total number of oxygens in the system ($X_{H_2O}/X_{H_2O} + 2X_{SiO_2}$). The solid vertical lines show the quartz saturation composition at 10 kbar and 1080 °C, above which the partitioning and average state of hydration are metastable (shown by dashed lines), as well as the maximum quartz solubility (~2 m, 0.034 mole fraction) that can be described by the monomer–dimer model of Newton and Manning (2002, 2003). The thin dashed line shows the average state of hydration of solute silica using the equilibrium constant determined by Stolper (1982).

This size may grow if, in addition to the equilibrium with monomers and dimers, equilibrium with Q^2 and small Q^3 species (rings, chains, and cages) is considered, due to the additional hydroxyl groups on these species that would not be available to create additional colloidal surface hydroxyls.

The calculated speciation of water as a function of composition (e.g., Fig. 7a) does not agree with experimental studies of water in quenched silicate glasses (e.g., Stolper, 1982). If the equilibrium constant determined by Stolper (1982) ($K_1^2 = 0.2$) were accurate for the system SiO_2–H_2O regardless of P or T, the average state of hydration of an aqueous silica solute in a solution at 2 m SiO_2 should be roughly 2 (Fig. 7b). Given that a solution at 2 m SiO_2 can be modeled as a collection of monomers and dimers (Newton and Manning, 2003, 2008), an average hydration state of 2 seems highly unlikely. However, when experiments were done on near-albitic wet glasses *in situ* (Shen and Keppler, 1995), much closer agreement is obtained. In fact, at 1080 °C and 10 kbar, the equilibrium constant obtained by Shen and Keppler is identical to that of the present model. Unfortunately, the assumptions contained in the model of Shen and Keppler – a linear variation of $\ln(K)$ with $1/T$ and a three-component ideal mixing model of H_2O, OH^-, and O^{2-} – cannot adequately describe the available quartz solubility data at 10 kbar. It is not clear if Na_2O–Al_2O_3–SiO_2–H_2O experiments are applicable to the SiO_2–H_2O system. The presence of alkali and aluminum ions may affect the formation of hydroxyl groups (Burnham and Davis, 1974; Mysen, 2010b), and therefore the general agreement between the model in the present study and experiments on near-albitic glasses may be in part fortuitous. It is clear, however, that K_1 varies with both temperature and pressure.

Fig. 8 shows a contour plot of the average hydration state of silica in an aqueous fluid in equilibrium with quartz. In general, increasing P at constant T along the quartz saturation surface will depolymerize the aqueous silica, increasing its average hydration state, though in certain regions (1000–1080 °C), quartz solubility increases rapidly enough with increasing P that the aqueous silica becomes more polymerized as P increases along the quartz saturation surface (Fig. 8). Increasing T along the quartz saturation surface always causes aqueous silica to polymerize; however, this is chiefly a consequence of the rapidly increasing concentration with rising T (Fig. 8). At a constant pressure and concentration, increasing T may lead to polymerization or depolymerization of aqueous silica, depending on the location in PTX space. Increasing P at a constant temperature and concentration, however, always causes depolymerization of aqueous silica.

The present model only provides an average hydration state for total dissolved silica. It is not possible to quantify abundances of individual Q^0 through Q^4 species. However, it should be noted that the monomer–dimer model of Newton and Manning (2002, 2003) is applicable to quartz saturated (or undersaturated) solutions with less than ~2 m silica, and the proportion of monomers, dimers, and higher polymers can be determined using the excess approach of Newton and Manning (2008). While polymerization (or average state of hydration) of silica as a function of composition will change as PT conditions change, our model generally predicts an average state of hydration between 3 and 4 for such dilute solutions (Fig. 7b). We do not necessarily conclude that these solutions are comprised entirely of monomers and dimers – it seems likely that there will be additional oligomers present, given the range of oligomers seen in relatively dilute alkaline silica solutions at ambient conditions (Knight et al., 2007) – but they could be energetically modeled as if they were comprised entirely of monomers and dimers.

Although it is not possible to quantify exact populations of the five categories of silica polymers with the present model, we can determine the minimum and maximum amount of polymerization at a given SiO_2 concentration. If all hydroxyl groups reside in monomers, then any remaining dissolved silica must be fully polymerized. Alternatively, if all bridging oxygens predicted by the model reside in dimers, any remaining dissolved silica must be monomeric. At 10 kbar and 1080 °C, for example, at least 15% and at most 60% of the silica must be polymerized at 2 m SiO_2. Clearly, however, both are unrealistic scenarios. In the former, the 15% polymerized silica would be entirely dissolved, yet completely dry, silica melt, which is highly unlikely. The latter scenario implies that 60% of the silica would be in dimers without a single further condensation reaction. While this is physically possible if it is assumed that only monomers and dimers can exist in solution, it is also highly unlikely. As SiO_2 concentration increases further, more bridging oxygens exist in solution than can possibly be accommodated in dimers, indicating that higher polymers must exist. The actual amount of polymerization (i.e., non-monomeric silica) is likely to be in between these extremes. This range is in good agreement with previous estimates of total silica polymerization (Newton and Manning, 2002, 2003, 2008; Gerya et al., 2005).

We have not considered the effects of hydrogen-bonded water to silica oligomers, if any; the hydration state of silica in this work is solely due to water reacting to form OH^- groups. At these high temperatures, it seems unlikely that there is much energetic difference between hydrogen-bonded and free water (e.g., Frantz et al., 1993, 1995, 2010a).

4.3. Subcritical phenomena

Although data along the wet melting curve (Kennedy et al., 1962) were not used in the model regression, the model predicts a wet melting temperature between 5 and 9 kbar of ~1066–1070 °C, and an upper critical end point at 1067 °C and 9.33 kbar (Fig. 4). The agreement with data from Kennedy et al. (1962) is significantly poorer than the agreement with the other data sets (Fig. 5); however, attempting to include the data from Kennedy et al. (1962) in the model regression led to unacceptable errors in fits to the other data sets. There is large experimental uncertainty in the Kennedy et al. (1962) data. At 1050 °C, Kennedy et al. (1962) determined quartz solubility to be 21 mol% silica at 9 kbar, and Newton and Manning (2008) determined quartz solubility to be 20 mol% at 10 kbar. Because of the topology of the isobaric solubility curves (Fig. 2), it is highly unlikely that quartz solubility would decrease or even stay constant when increasing P from 9 to 10 kbar at 1050 °C. In light of these uncertainties, we consider the model wet melting temperature and upper critical end point to be in reasonable agreement with Kennedy et al. (1962).

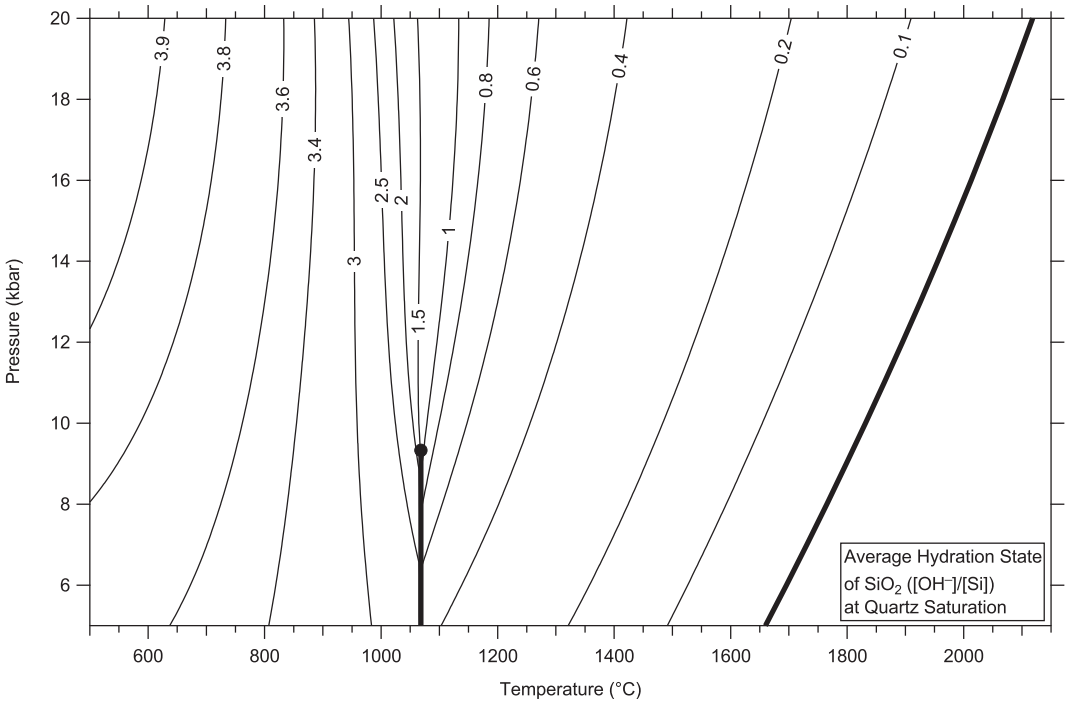

Fig. 8. Average state of hydration (N_{OH^-}/X_s ratio) of solute silica at quartz saturation as a function of pressure and temperature. Bold curves are the same as in Fig. 4. The lighter solid curves are contours of constant average state of hydration, where 4 corresponds to entirely monomeric silica, and 0 corresponds to fully polymerized dry silica melt.

Little work has been done to determine water solubility in pure silica melts at pressures below the upper critical end point; our model is therefore mostly calibrated on the H_2O-rich side of the system. However, there is one data point (Holtz et al., 2000) within the applicable pressure and temperature ranges of our model that can be compared. At 1200 °C and 6 kbar, Holtz et al. (2000) determined water solubility to be approximately 22.5 mol%, while our model predicts water solubility to be 18.4 mol%. We consider these values to be in good agreement, especially in light of the fact that no subcritical, silica-rich data were used in the regression analysis.

4.4. Thermodynamic derivatives

The stable or metastable dissolution of silica liquid in SiO_2–H_2O solutions can be expressed as

$$SiO_{2(liq)} = SiO_{2(liq,soln)} \tag{13}$$

With our adopted standard state for aqueous silica of unit mole fraction of dry liquid SiO_2, the equilibrium constant of Eq. (13) may be expressed as the activity of aqueous silica at a given P, T, and X_s, given by Eq. (7). The partial molar entropy and volume of reaction (13) can thus be derived via the following equations:

$$-R\left(\frac{\partial T\ \ln(a_{s,l})}{\partial T}\right)_{P,X_s} = \Delta\overline{S}_{13} \tag{14}$$

$$RT\left(\frac{\partial\ \ln(a_{s,l})}{\partial P}\right)_{T,X_s} = \Delta\overline{V}_{13} \tag{15}$$

The reaction from quartz to aqueous silica is given by

$$SiO_{2(qtz)} = SiO_{2(liq,soln)} \tag{16}$$

The standard Gibbs free energy of Eq. (6) can be expressed as the sum of dry quartz melting (Eq. (6)), and the standard Gibbs free energy of Eq. (13). The molar entropy and volume of dry quartz melting can be obtained by differentiating Eq. (6) with T and P respectively, giving $\Delta S^\circ_{Q\text{–}L} = 5.53$ J/K (a trivial result, as this value was previously assumed as the entropy of quartz melting) and $\Delta V^\circ_{Q\text{–}L} = \left(\frac{dT_{melt}}{dP}\right)\Delta S^\circ_{Q\text{–}L}$ J/bar. The standard molar entropy of reaction 16 (Fig. 9) is therefore given by the sum of Eq. (14) and $\Delta S^\circ_{Q\text{–}L}$. The standard molar volume of reaction 16 (Fig. 10) is likewise given by the sum of Eq. (15) and $\Delta V^\circ_{Q\text{–}L}$. The standard partial molar volume and entropy of aqueous silica at the P and T of interest is given by simply adding the standard molar volume or entropy of reaction (16) to the standard molar volume or entropy of quartz, which can be readily obtained using a thermodynamic database such as Holland and Powell (1998).

Of particular note in Fig. 10 is the contour corresponding to $\Delta\overline{V}_{16} = 0$. At T lower than this contour, the volume change of the reaction is negative, and at T above this contour, the volume change is positive. This provides a convenient division of supercritical aqueous silicate – at temperatures below the $\Delta\overline{V}_{16} = 0$ contour, SiO_2 volume decreases as it is transferred from quartz to aqueous silica, while above those temperatures, SiO_2 volume increases as it is transferred from quartz to a hydrous silicate melt. This contour may therefore represent a better "extension" of the

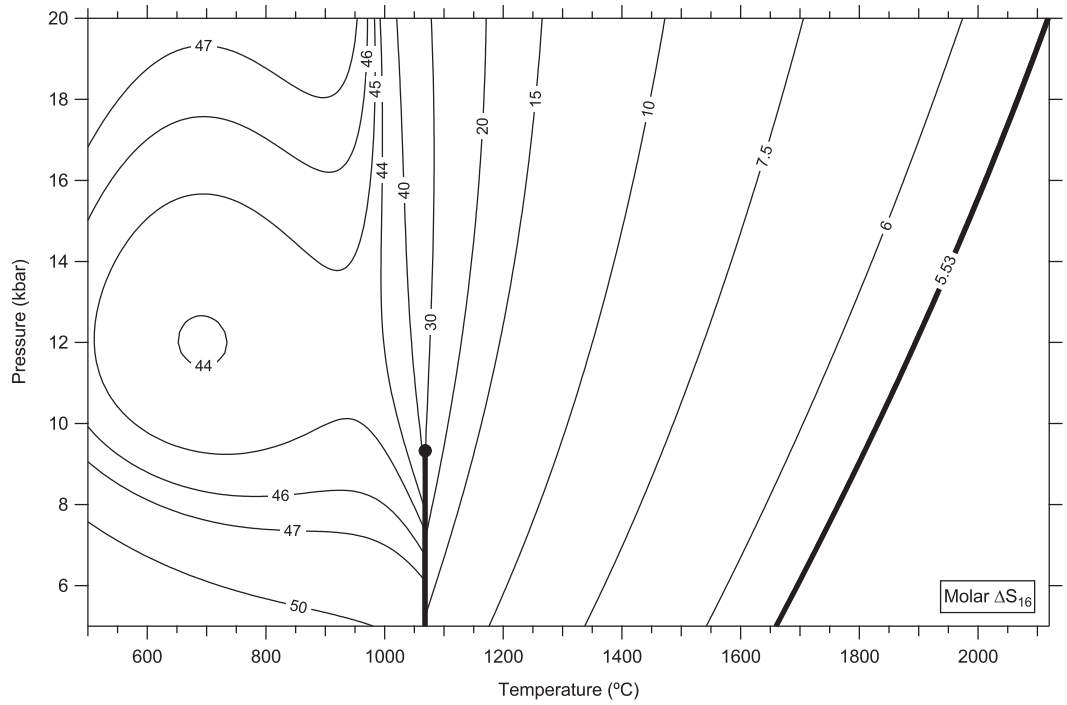

Fig. 9. Standard molar entropy of reaction 16 as a function of pressure and temperature. Bold curves are the same as in Fig. 4. The lighter solid curves are contours of constant standard molar entropy of reaction 16 in J/K. The increase in partial molar entropy at high P and low T is most likely due to increased depolymerization (N_{OH^-}/X_s ratio) at these conditions.

hydrous melting curve than the contour corresponding to the critical composition advocated by Hack et al. (2007a,b).

The molar volume (and therefore, density) and entropy of an aqueous fluid in equilibrium with quartz is obtained

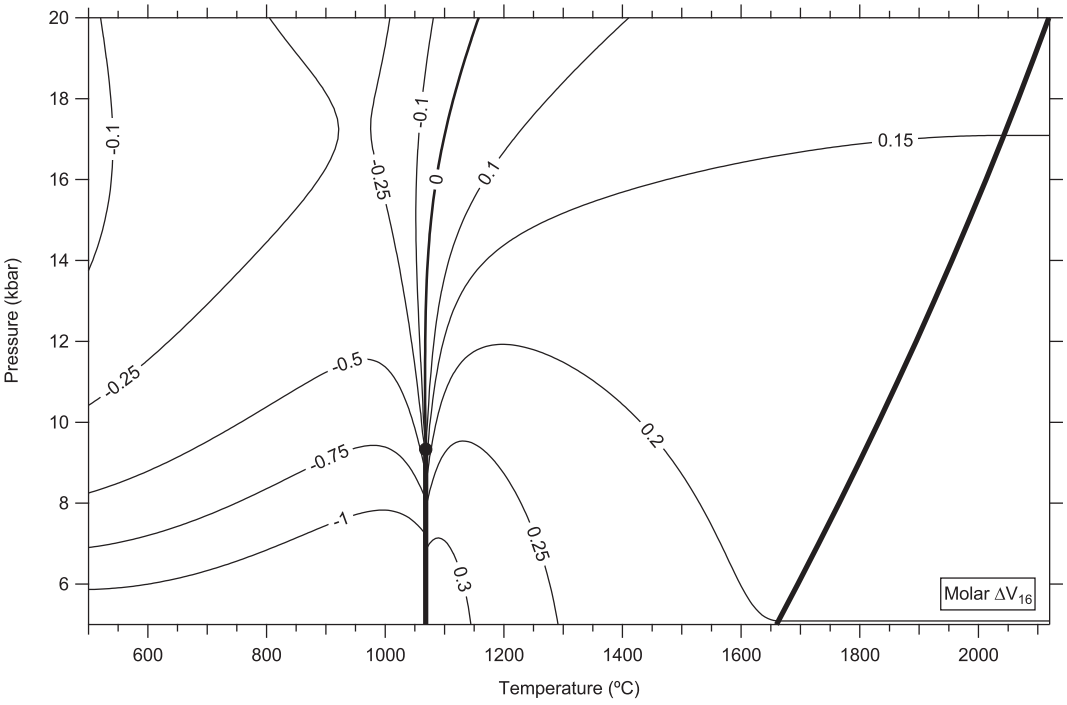

Fig. 10. Standard molar volume of reaction 16 as a function of pressure and temperature. Bold curves are the same as in Fig. 4. The lighter solid curves are contours of constant standard molar volume of reaction 16 in J/bar. The thin bolded curve is the contour of zero standard molar volume of reaction 16.

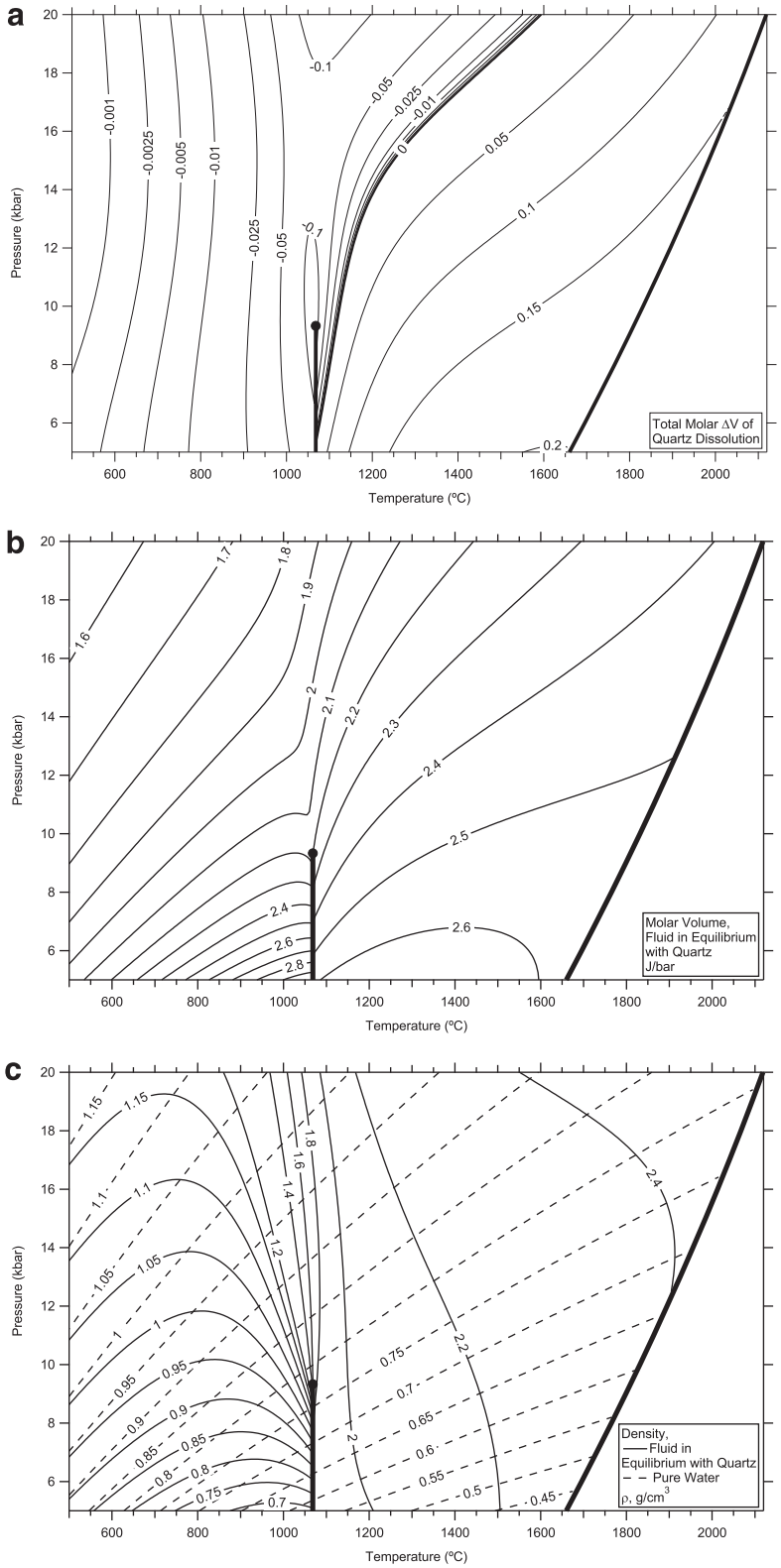

Fig. 11. (a) Molar volume change between $X_s SiO_{2,qtz} + (1 - X_s)H_2O$ and the fluid in equilibrium with quartz, where X_s is the quartz saturation composition, as a function of pressure and temperature, in J/bar. (b) Molar volume of fluid in equilibrium with quartz as a function of pressure and temperature, in J/bar. (c) Density of fluid in equilibrium with quartz and density of pure water as a function of pressure and temperature, in g/cm^3. Bold curves in all contour plots are the same as in Fig. 4.

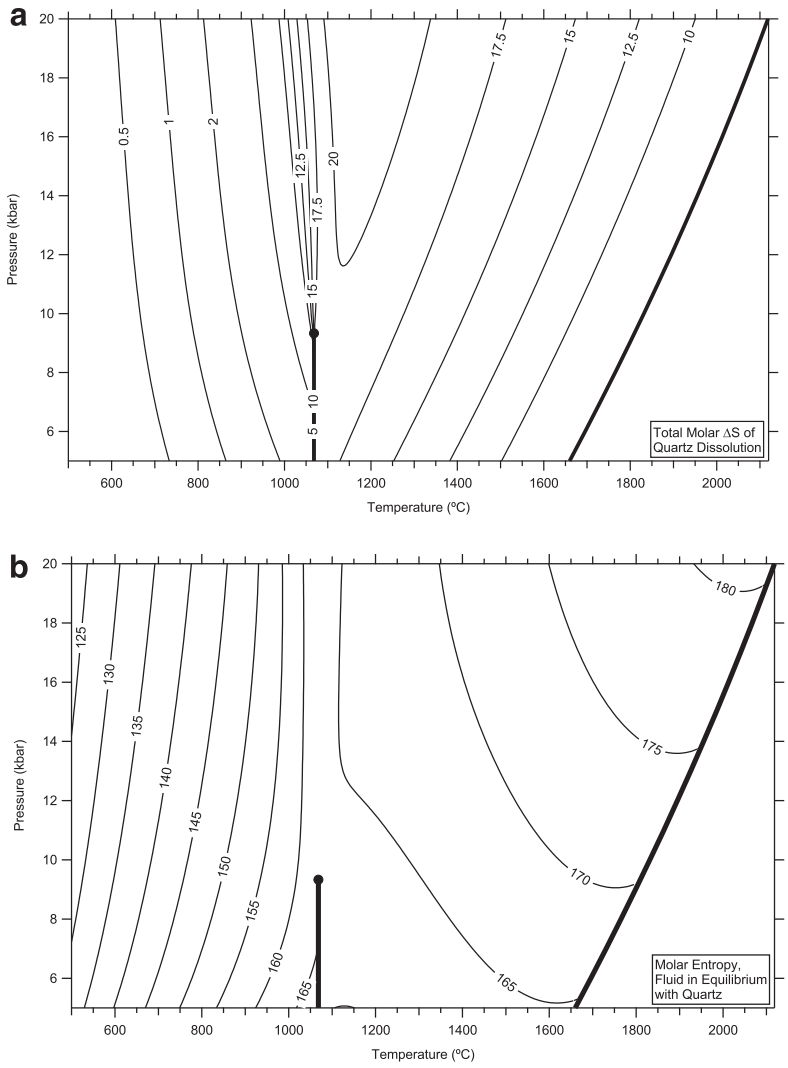

Fig. 12. (a) Molar entropy change between $X_s SiO_{2,qtz} + (1 - X_s)H_2O$ and the fluid in equilibrium with quartz, where X_s is the quartz saturation composition, and (b) Molar entropy of fluid in equilibrium with quartz as a function of pressure and temperature, in J/K. Bold curves are the same as in Fig. 4.

by performing a similar analysis of the activity of water, and then weighting each partial molar quantity by the quartz saturation composition. It should be noted here that while a comparison could be made between the model partial molar volume of water and experimental measurements of the partial molar volume in silicate glasses (Richet and Polian, 1998), it would not be a direct comparison, as the experimental measurement was only done on quenched glasses at ambient conditions. The present model reports partial molar volumes of water that are both more and less dense than the experimentally measured value of 1.2 J/bar, depending on the pressure and temperature. Fig. 11 shows (a) the difference in volume between quartz + pure water and a hydrous silicate fluid, (b) the molar volume of a fluid in equilibrium with quartz, and (c) the density of a fluid in equilibrium with quartz, compared to the density of pure water. The contour corresponding to $\Delta\overline{V} = 0$ in Fig. 11a shows that, in a system assumed to be isochoric (e.g., a diamond anvil cell), as temperature is increased from ambient T to this contour, the pressure will increase slightly less than it would under the assumption that the fluid volume is equal to the sum of the volumes of water and quartz. Fig. 12 shows (a) the total change in entropy from quartz + pure water to a hydrous silicate fluid, which naturally (due to the maximum of ideal mixing entropy at $X = 0.5$) rises to a maximum for intermediate fluids, and (b) the molar entropy of a fluid in equilibrium with quartz.

Once the molar volume and entropy of the fluid phase in equilibrium with quartz are known, thermodynamic second derivatives can be computed. Fig. 13 shows (a) the thermal expansion parameter, α, (b) the isothermal compressibility β, and (c) the isobaric heat capacity, C_P, of a fluid in equilibrium with quartz as well as for pure water as a function of temperature and pressure. It should be noted that these derivatives depend heavily on the volume and entropy of quartz as calculated from the Holland and Powell (1998)

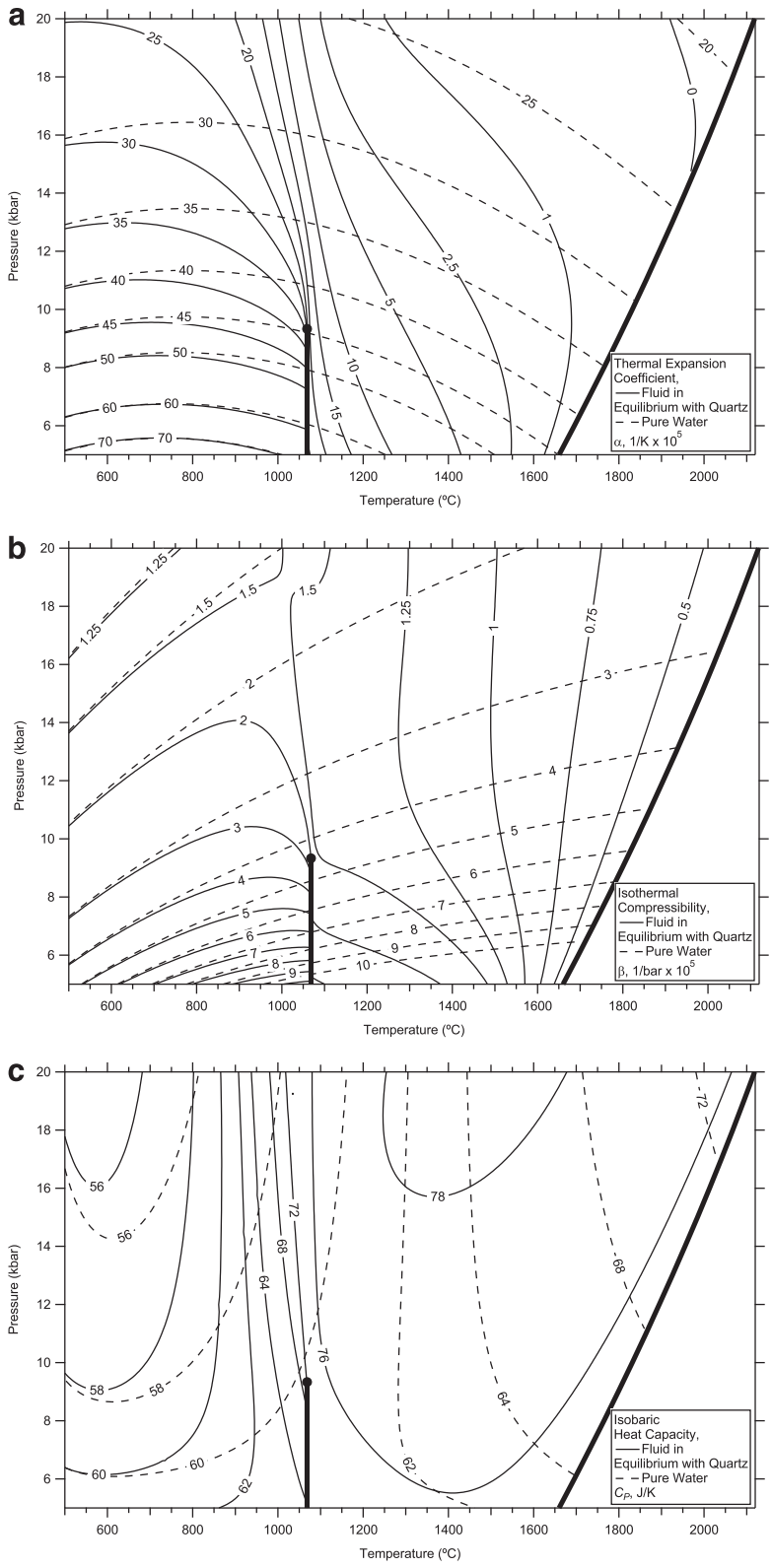

Fig. 13. (a) Coefficient of thermal expansion, $\alpha \times 10^5$ (1/K), (b) the isothermal compressibility $\beta \times 10^5$ (1/bar), and (c) the isobaric heat capacity, C_P (J/K), of a fluid in equilibrium with quartz (solid lines) and pure water (dashed lines) as a function of temperature and pressure. Bold curves are the same as in Fig. 4.

data set (2002 update), and therefore care must be taken to correct for the entropy and volume increase of the transition from α to β quartz. Fig. 13 has been corrected in this manner; without the correction, a discontinuity in the contour lines would exist at the α–β quartz transition (Fig. 1). This dependence on the Holland and Powell (1998) data set (2002 update) is also the reason for the negative coefficient of thermal expansion above ~1900 °C and ~15 kbar (Fig. 13a). This phenomenon is well known for quartz at these conditions, but it is unclear if molten silica exhibits the same behavior, or if Eq. (6) needs to be refined to reflect more accurately the properties of molten silica.

The comparison between the properties of a fluid in equilibrium with quartz and pure H_2O in Figs. 11c and 13 shows that the assumption that natural fluids at high T and P can be approximated by the properties of pure H_2O can lead to significant error. This is supported by a recent investigation of aqueous silicate fluids using independent pressure calibration in the diamond anvil cell by Mysen (2010a). The properties of natural fluids will deviate significantly at high T and P from the properties of pure H_2O, with the deviation increasing as the amount of total dissolved solids increases in the supercritical region.

4.5. Limitations

As mentioned previously, while this model gives an average hydration state of solute silica, it cannot predict populations of the five major categories of silica polymers. The parameters describing the Gibbs free energy of the depolymerization reaction should change if the model describing the weak interactions changes (e.g., using a regular or subregular solution of three components, rather than a subregular solution of two components). Thus while this model describes silica solubility quite well over a large PT range, the average state of hydration of solute silica is merely a prediction, and may change slightly as the model is refined and/or extended to lower or higher pressures and lower temperatures.

Another limitation is that there is no guarantee that the least-squares regression gives a unique solution; the error surface is highly irregular, and the choice of initial guesses for each of the parameters is very important. It may be possible to use existing algorithms to find a global error minimum over all thirteen parameters, if a robust forward model to calculate an accurate solubility given a set of parameters, pressure, and temperature can be developed. The procedure to calculate quartz solubility given a set of parameters, pressure, and temperature is given in Appendix A, but verification that the calculated solubility is correct (for example, verifying that the calculated solubility lies outside of a miscibility gap) has so far been done solely by inspection.

The metastable free energy of melting of quartz is assumed to be given by a very simple expression (Eq. (6)). This cannot be a perfectly valid assumption over the entire PT range considered in this paper, as there is a Gibbs free energy change associated with the transition from α to β quartz. Refining Eq. (6), either to account for this transition or to incorporate a generally more sophisticated expression for the standard Gibbs free energy of dry molten silica, may change the model considerably.

5. CONCLUSIONS

The new experimental quartz solubility results provide accurate determinations of the 15 and 20 kbar isobars of quartz saturation. These data, in conjunction with previously determined quartz solubility data sets, constrain a modified subregular solution model that describes quartz solubility, melting behavior and critical phenomena in addition to making predictions of activity–concentration relations and speciation over a large PT range. The model suggests that speciation of aqueous silica can be thought of in the same way that speciation of water in silicate melts is; as a mixture of free H_2O, terminal OH^- groups, and bridging oxygens (O^{2-}). Modeled oxygen speciation in the SiO_2–H_2O system is in general agreement with *in situ* measurements of oxygen speciation in near-albitic glasses, and estimates of silica polymerization are in general agreement with previous studies. The current model could be tested and/or refined with additional experimentation, including accurate determination of quartz solubility at $P < 5$ kbar and $T > 900$ °C, and along the hydrothermal melting curve. *In situ* measurement of oxygen speciation in pure SiO_2–H_2O glasses would be even better, as it would allow a single component of the model ΔG_1° to be tested and fitted, putting further constraints on the remainder of the mixing model. This last, however, may be difficult to achieve, given the high melting temperature of hydrous SiO_2 (especially compared to the melting temperature of hydrous albite) and temperature limits in externally heated diamond anvil cells.

ACKNOWLEDGMENTS

The authors are indebted to Bob Newton for many insightful and stimulating discussions of thermodynamics. We also thank B. Mysen, H. Keppler, S. Jahn, and K. Mibe for helpful reviews of the manuscript. Supported by NSF EAR 1049901. Portions of this work were performed under the auspices of the US Department of Energy by Lawrence Livermore National Laboratory under Contract DE-AC52-07NA27344.

APPENDIX A

The calculation of quartz solubility given a P and T of interest must be done numerically, as there is no closed-form solution to Eq. (5), text. Combining Eqs. (7) and (9), text, so that $RT\ln a_{s,l}^{Q} = RT\ln a_{s,l}$, we obtain

$$(T - T_{melt})\Delta S_{Q\text{–}L}^\circ = RT\ln X_s + (1 - X_s)^2(W_s + 2X_s(W_h - W_s)) - \Delta G_1^\circ\left[X_{OH^-} + (1 - X_s)\frac{\partial X_{OH^-}}{\partial X_s}\right] \quad \text{(A1)}$$

where T_{melt} is obtained from Jackson (1976), $\Delta S_{Q\text{–}L}^\circ$ is a constant 5.53 J/K, ΔG_1°, W_s, and W_h are given by Eqs. (10)–(12), text, respectively, and X_{OH^-} and $\frac{\partial X_{OH^-}}{\partial X_s}$ are given as follows:

$$X_{OH^-} = \frac{\frac{(X_s+1)}{2} - \sqrt{\left(\frac{X_s+1}{2}\right)^2 - 4\left(\frac{1}{4} - \frac{1}{K_1^2}\right)(2X_s - 2X_s^2)}}{2\left(\frac{1}{4} - \frac{1}{K_1^2}\right)} \quad (A2)$$

$$\frac{\partial X_{OH^-}}{\partial X_s} = \frac{K_1^2\left(\sqrt{\frac{K_1^2(1-3X_s)^2 - 32(X_s-1)X_s}{K_1^2}} - 9X_s + 3\right) + 32X_s - 16}{(K_1^2 - 4)\sqrt{\frac{K_1^2(1-3X_s)^2 - 32(X_s-1)X_s}{K_1^2}}} \quad (A3)$$

where K_1, as per Eq. (2), text, is given by

$$K_1 = \exp\left(\frac{-\Delta G_1^\circ}{RT}\right) \quad (A4)$$

Eq. (A2) is simply the solution of Eq. (2), text, for X_{OH^-}, and Eq. (A3) is the derivative of Eq. (A2) with respect to X_s. If K_1 happens to equal 2 (it never does, in this model, but we include it here for completeness), X_{OH^-} and $\frac{\partial X_{OH^-}}{\partial X_s}$ are given by

$$X_{OH^-} = \frac{4(1 - X_s)(X_s)}{(1 + X_s)} \quad (A5)$$

$$\frac{\partial X_{OH^-}}{\partial X_s} = \frac{-4(X_s^2 + 2X_s - 1)}{(1 + X_s)^2} \quad (A6)$$

A simple numerical solver will accurately solve Eq. (A1) for X_s. However, care must be taken in the subcritical region ($T < 1070$ °C or $P < 9330$ bar), as a stable or metastable miscibility gap will exist and therefore more than one value for X_s will satisfy Eq. (A1). The miscibility gap between compositions X_1 and X_2 can be determined by solving, numerically and simultaneously, the following equations for X_1 and X_2 (where $X_1 \neq X_2$):

$$\begin{aligned} &RT\ln X_1 + (1 - X_1)^2(W_s + 2X_1(W_h - W_s)) \\ &\quad - \Delta G_1^\circ\left[X_{OH^-}|_{X_1} + (1 - X_1)\frac{\partial X_{OH^-}}{\partial X_s}\bigg|_{X_1}\right] \\ &\quad = RT\ln X_2 + (1 - X_2)^2(W_s + 2X_2(W_h - W_s)) \\ &\quad - \Delta G_1^\circ\left[X_{OH^-}|_{X_2} + (1 - X_2)\frac{\partial X_{OH^-}}{\partial X_s}\bigg|_{X_2}\right] \end{aligned} \quad (A7)$$

$$\begin{aligned} &RT\ln(1-X_1) + X_1^2(W_h + 2(1-X_1)(W_s - W_h)) \\ &\quad - \Delta G_1^\circ\left[X_{OH^-}|_{X_1} - X_1\frac{\partial X_{OH^-}}{\partial X_s}\bigg|_{X_1}\right] \\ &\quad = RT\ln(1-X_2) + X_2^2(W_h + 2(1-X_2)(W_s - W_h)) \\ &\quad - \Delta G_1^\circ\left[X_{OH^-}|_{X_2} - X_2\frac{\partial X_{OH^-}}{\partial X_s}\bigg|_{X_2}\right] \end{aligned} \quad (A8)$$

Eqs. (A7) and (A8) simply equate the activity of silica (Eq. (7), text) at X_1 and X_2, and water (Eq. (8), text) at X_1 and X_2, respectively. The true solubility will be the greatest possible value for X_s outside this miscibility gap, unless each side of Eq. (A7) is also equal to $RT\ln a_{s,l}^{Q}$, which defines the hydrous melting temperature of quartz and the compositions of the two fluids in equilibrium with quartz at the melting temperature.

REFERENCES

Anderson G. M. and Burnham C. W. (1965) Solubility of quartz in supercritical water. *Am. J. Sci.* **263**, 494–511.

Antignano A. and Manning C. E. (2008) Rutile solubility in H_2O, $H_2O - SiO_2$, and $H_2O - NaAlSi_3O_8$ fluids at 0.7–2.0 GPa and 700–1000 °C: Implications for mobility of nominally insoluble elements. *Chem. Geol.* **255**, 283–293.

Audétat A. and Keppler H. (2004) Viscosity of fluids in subduction zones. *Science* **303**, 513–516.

Bureau H. and Keppler H. (1999) Complete miscibility between silicate melts and hydrous fluids in the upper mantle: experimental evidence and geochemical implications. *Earth Planet. Sci. Lett.* **165**, 187–196.

Burnham C. W. and Davis N. F. (1974) Role of H_2O in silicate melts: 2. Thermodynamic and phase relations in system $NaAlSi_3O_8$–H_2O to 10 kilobars, 700 degrees centigrade to 1100 degrees centigrade. *Am. J. Sci.* **274**, 902–940.

Cohen L. H. and Klement W. (1967) High-low quartz inversion – determination to 35 kilobars. *J. Geophys. Res.* **72**, 4245–4251.

Dolejs D. and Manning C. E. (2010) Thermodynamic model for mineral solubility in aqueous fluids: theory, calibration and application to model fluid-flow systems. *Geofluids* **10**, 20–40.

Doltsinis N. L., Burchard M., Maresch W. V., Boese A. D. and Fockenberg T. (2007) Ab initio molecular dynamics study of dissolved SiO_2 in supercritical water. *J. Theor. Comput. Chem.* **6**, 49–62.

Fournier R. O. and Potter R. W. (1982) An equation correlating the solubility of quartz in water from 25 °C to 900 °C at pressures up to 10,000 bars. *Geochim. Cosmochim. Acta* **46**, 1969–1973.

Frantz J. D., Dubessy J. and Mysen B. O. (1993) An optical cell for Raman spectroscopic studies of supercritical fluids and its application to the study of water to 500 °C and 2000 bar. *Chem. Geol.* **106**, 9–26.

Gerya T. V. et al. (2005) Thermodynamic modeling of solubility and speciation of silica in H_2O–SiO_2 fluid up to 1300 degrees C and 20 kbar based on the chain reaction formalism. *Eur. J. Mineral.* **17**, 269–283.

Gorbaty Y. E. and Kalinichev A. G. (1995) Hydrogen Bonding in Supercritical Water.1. Experimental Results. *J. Phys. Chem.* **99**, 5336–5340.

Hack A. C., Hermann J. and Mavrogenes J. A. (2007a) Mineral solubility and hydrous melting relations in the deep earth: analysis of some binary A-H_2O system pressure–temperature–composition topologies. *Am. J. Sci.* **307**, 833–855.

Hack A. C., Thompson A. B. and Aerts M. (2007b) Phase relations involving hydrous silicate melts, aqueous fluids, and minerals. *Fluid–Fluid Interact.* **65**, 129–185.

Hack A. C. and Thompson A. B. (2011) Density and viscosity of hydrous magmas and related fluids and their role in subduction zone processes. *J. Petrol.* **52**, 1333–1362.

Hermann J. and Spandler C. J. (2008) Sediment melts at sub-arc depths: an experimental study. *J. Petrol.* **49**, 717–740.

Holland T. J. B. and Powell R. (1998) An internally consistent thermodynamic data set for phases of petrological interest. *J. Metamorph. Geol.* **16**, 309–343.

Holtz F., Roux J., Behrens H. and Pichavant M. (2000) Water solubility in silica and quartzofeldspathic melts. *Am. Mineral.* **85**, 682–686.

Hunt J. D., Kavner A., Schauble E. A., Snyder D. and Manning C. E. (2011) Polymerization of aqueous silica in H_2O–K_2O solutions at 25–200 °C and 1 bar to 20 kbar. *Chem. Geol.* **283**, 161–170.

Iler R. K. (1979) *The Chemistry of Silica*. Wiley.

Jackson I. (1976) Melting of silica isotypes SiO_2, BeF_2 and GeO_2 at elevated pressures. *Phys. Earth Planet. In.* **13**, 218–231.

Kennedy G. C. (1950) A portion of the system silica–water. *Econ. Geol.* **45**, 629–653.

Kennedy G. C., Heard H. C., Wasserburg G. J. and Newton R. C. (1962) Upper 3-phase region in system SiO_2–H_2O. *Am. J. Sci.* **260**, 501–521.

Kessel R., Ulmer P., Pettke T., Schmidt M. W. and Thompson A. B. (2005a) The water–basalt system at 4 to 6 GPa: phase relations and second critical endpoint in a K-free eclogite at 700 to 1400 degrees C. *Earth Planet. Sci. Lett.* **237**, 873–892.

Kessel R., Schmidt M. W., Ulmer P. and Pettke T. (2005b) Trace element signature of subduction zone fluids, melts, and supercritical liquids at 120–180 km depth. *Nature* **437**, 724–727.

Knight C. T. G., Balec R. J. and Kinrade S. D. (2007) The structure of silicate anions in aqueous alkaline solutions. *Angew. Chem. Int. Ed.* **46**, 8148–8152.

Manning C. E. (1994) The solubility of quartz in H_2O in the lower crust and upper-mantle. *Geochim. Cosmochim. Acta* **58**, 4831–4839.

Manning C. E. (2004) The chemistry of subduction-zone fluids. *Earth Planet. Sci. Lett* **223**, 1–16.

Manning C. E., Antignano A. and Lin H. A. (2010) Premelting polymerization of crustal and mantle fluids, as indicated by the solubility of albite plus paragonite plus quartz in H_2O at 1 GPa and 350–620 degrees C. *Earth Planet. Sci. Lett.* **292**, 325–336.

Manning C. E. and Boettcher S. L. (1994) Rapid-quench hydrothermal experiments at mantle pressures and temperatures. *Am. Mineral.* **79**, 1153–1158.

Mibe K., Kanzaki M., Kawamoto T., Matsukage K. N., Fei Y. and Ono S. (2004) Determination of the second critical end point in silicate–H_2O systems using high-pressure and high-temperature X-ray radiography. *Geochim. Cosmochim. Acta* **68**, 5189–5195.

Mibe K., Kanzaki M., Kawamoto T., Matsukage K. N., Fei Y. and Ono S. (2007) Second critical endpoint in the peridotite–H_2O system. *J. Geophys. Res.* **112**, B03201.

Mibe K., Kawamoto T., Matsukage K. N., Fei Y. and Ono S. (2011) Slab melting versus slab dehydration in subduction-zone magmatism. *Proc. Natl. Acad. Sci. USA* **108**, 8177–8182.

Mysen B. O. (1998) Interaction between aqueous fluid and silicate melt in the pressure and temperatures regime of the Earth's crust and upper mantle. *Neues. Jb. Miner. Abh.* **172**, 227–244.

Mysen B. O. (2010a) Speciation and mixing behavior of silica-saturated aqueous fluid at high temperature and pressure. *Am. Mineral.* **95**, 1807–1816.

Mysen B. O. (2010b) Structure of H_2O-saturated peralkaline aluminosilicate melt and coexisting aluminosilicate-saturated aqueous fluid determined in-situ to 800 °C and 800 MPa. *Geochim. Cosmochim. Acta* **74**, 4123–4139.

Nakamura Y. (1974) The system SiO_2–H_2O–H_2 at 15 kbar. *Carnegie Inst. Wash. Publ.* **73**, 259–263.

Newton R. C. and Manning C. E. (2000) Quartz solubility in $H_2O - NaCl$ and $H_2O - CO_2$ solutions at deep crust-upper mantle pressures and temperatures: 2–15 kbar and 500–900 ° C. *Geochim. Cosmochim. Acta.* **64**, 2993–3005.

Newton R. C. and Manning C. E. (2002) Solubility of enstatite plus forsterite in H_2O at deep crust/upper mantle conditions: 4 to 15 kbar and 700 to 900 degrees C. *Geochim. Cosmochim. Acta* **66**, 4165–4176.

Newton R. C. and Manning C. E. (2003) Activity coefficient and polymerization of aqueous silica at 800 degrees C, 12 kbar, from solubility measurements on SiO_2-buffering mineral assemblages. *Contrib. Mineral. Petrol.* **146**, 135–143.

Newton R. C. and Manning C. E. (2006) Solubilities of corundum, wollastonite and quartz in H_2O–NaCl solutions at 800 degrees C and 10 kbar: interaction of simple minerals with brines at high pressure and temperature. *Geochim. Cosmochim. Acta* **70**, 5571–5582.

Newton R. C. and Manning C. E. (2007) Solubility of grossular, $Ca_3Al_2Si_3O_{12}$, in H_2O–NaCl solutions at 800 degrees C and 10 kbar, and the stability of garnet in the system $CaSiO_3$–Al_2O_3–H_2O–NaCl. *Geochim. Cosmochim. Acta* **71**, 5191–5202.

Newton R. C. and Manning C. E. (2008) Thermodynamics of SiO_2–H_2O fluid near the upper critical end point from quartz solubility measurements at 10 kbar. *Earth Planet. Sci. Lett.* **274**, 241–249.

Richet P., Bottinga Y., Denielou L., Petitet J. P. and Tequi C. (1982) Thermodynamic properties of quartz, cristobalite and amorphous SiO_2 – drop calorimetry measurements between 1000-K and 1800-K and a review from 0-K to 2000-K. *Geochim. Cosmochim. Acta* **46**, 2639–2658.

Richet P. and Polian A. (1998) Water as a dense icelike component in silicate glasses. *Science* **281**, 396–398.

Shen A. and Keppler H. (1995) Infrared spectroscopy of hydrous silicate melts to 1000 degrees C and 10 kbar: direct observation of H_2O speciation in a diamond-anvil cell. *Am. Mineral.* **80**, 1335–1338.

Shen A. H. and Keppler H. (1997) Direct observation of complete miscibility the albite–H_2O system. *Nature* **385**, 710–712.

Singh R. N., Jha I. S. and Pandey D. K. (1993) Thermodynamics of liquid Mg–Sn alloys. *J. Phys.: Condens. Mat.* **5**, 2469–2478.

Sowerby J. R. and Keppler H. (2002) The effect of fluorine, boron and excess sodium on the critical curve in the albite–H_2O system. *Contrib. Mineral. Petrol.* **143**, 32–37.

Stalder P., Ulmer P., Thompson A. B. and Gunther D. (2000) Experimental approach to constrain second critical end points in fluid/silicate systems: near-solidus fluids and melts in the system albite–H_2O. *Am. Mineral.* **85**, 68–77.

Stewart D. B. (1967) Four-phase curve in the system $CaAl_2Si_2O_8$–SiO_2–H_2O between 1 and 10 kilobars. *Schweiz. Miner. Petrog.* **47**, 35–59.

Stolper E. (1982) Water in silicate-glasses – an infrared spectroscopic study. *Contrib. Mineral. Petrol.* **81**, 1–17.

Tropper P. and Manning C. E. (2007a) The solubility of corundum in H_2O at high pressure and temperature and its implications for Al mobility in the deep crust and upper mantle. *Chem. Geol.* **240**, 54–60.

Tropper P. and Manning C. E. (2007b) The solubility of fluorite in H_2O and H_2O–NaCl at high pressure and temperature. *Chem. Geol.* **242**, 299–306.

Walther J. V. and Helgeson H. C. (1977) Calculation of thermodynamic properties of aqueous silica and solubility of quartz and its polymorphs at high-pressures and temperatures. *Am. J. Sci.* **277**, 1315–1351.

Zotov N. and Keppler H. (2000) In-situ Raman spectra of dissolved silica species in aqueous fluids to 900°C and 14 kbar. *Am. Min.* **85**, 600–603.

Zotov N. and Keppler H. (2002) Silica speciation in aqueous fluids at high pressures and high temperatures. *Chem. Geol.* **184**, 71–82.

Associate editor: Bjorn Mysen